

Surface Characteristics of Anodized Ti-3wt%, 20wt%, and 40wt%Nb Alloys

Y. M. Ko, H. C. Cho[†], S. H. Jang, and T. H. Kim

Chosun University, 2nd stage of Korea 21 for College of Dentistry, Gwangju, South Korea
(Received April 30, 2007; No Revision; Accepted July 21, 2009)

In biomedical implants and dental fields, titanium has been widely utilized for excellent corrosion resistance and biocompatibility. However, Ti and its alloys are nonbioactive after being implanted in bone. In this study, for the purpose of improvement in biocompatibility the anodic TiO₂ layer on Ti-xNb alloys were fabricated by electrochemical method in phosphate solution, and the effect of Nb content on the pore size, the morphology and crystallinity of Ti oxide layer formed by the anodic oxidation method was investigated. The Ti containing Nb up to 3 wt%, 20 wt% and 40 wt% were melted by using a vacuum furnace. The sample were cut, polished, and homogenized for 24 hr at 1050 °C for surface roughness test and anodizing. Titanium anodic layer was formed on the specimen surface in an electrolytic solution of 1 M phosphoric acid at constant current densities (30 mA/cm²) by anodizing method. Microstructural morphology, crystallinity, composition, and surface roughness of oxide layer were observed by FE-SEM, XRD, EDS, and roughness tester, respectively. The structure of alloy was changed from α -phase to β -phase with increase of Nb content. From XRD results, the structure of TiO₂ formed on the Ti-xNb surface was anatase, and no peaks of Nb₂O₅ or other Nb oxide were detected suggesting that Nb atoms are dispersed in TiO₂-based solid solution. Surface roughness test and SEM results, pore size formed on surface and surface roughness decreased as Nb content increased. From the line analysis results, intensity of Ti peak was high in the center of pore, whereas, intensity of O peak was high in the outside of pore center.

Keywords : corrosion characteristics, anodized, constant current densities

1. Introduction

Pure titanium and Ti-6Al-4V ELI alloys have been widely used as permanent implant materials in the replacement of damaged hard tissues, such as in artificial hip joints and dental implants, due to their excellent corrosion resistance, high specific strength and reasonable biocompatibility among the metal-based biomaterials. These properties are achieved by a thin titanium oxide based layer that is always present on these alloys surface.^{1),2)} Thick and dense oxide layers result in lower passive currents and correspondingly lower metal ion release into the body fluids. Moreover, the interaction of tissues and cells with Ti alloy implants is largely determined by the composition and microstructure of the oxide layer. However, Ti and its alloys are non-bioactive after being implanted in bone. Thus, for further improvement in biocompatibility the various implant surface modifications have been investigated. These surface modifications have included sandblasting,³⁾

acid etching,⁴⁾ combination of sandblasting and acid etching,⁵⁾ sol-gel technique,⁶⁾⁻⁸⁾ deposition of Ti coatings using plasma spraying, and deposition of calcium phosphate or hydroxyapatite coatings.⁹⁾⁻¹³⁾ In addition, as far as human body applications of these materials are concerned, surface modification is indispensable for the latter alloy because vanadium is known to be a toxic element, both in the elemental state and in its oxide form, V₂O₅, even though these alloys have been registered in ASTM standards for biomedical applications.

To solve these problems, new Ti-based alloys with biocompatible elements such as Nb, Zr, Ta, Sn, and without toxic elements such as V, Al, Ni, have been developed in order to match the mechanical and physical properties of the Ti-6Al-4V.^{14),15)}

In the present study, we chose Nb as a binary alloying element because it has excellent biocompatibility and be expected to act as a β -stabilizer. For the purpose of improvement in biocompatibility, the anodic TiO₂ layer on Ti-xNb alloys were fabricated by electrochemical method in phosphate solution, and then the effect of Nb content

[†] Corresponding author: hcchoe@chosun.ac.kr

on the pore size, the morphology and crystallinity of Ti oxide layer formed by the anodic oxidation method was investigated.

2. Experimental

2.1 Materials

The purities of the starting raw materials were 99.99% for Ti and 99.9% for Nb. A series of Ti-xNb alloys (3, 20 and 40%) (in this study, all the percentages are shown in weight%) were prepared. Small alloy buttons of 30 mm in diameter were prepared by arc melting on a water-sealed copper hearth under an argon gas atmosphere with a non-consumable tungsten electrode. Each button ingots was melted six times by inverting the metal to ensure homogeneous melting. The button ingots were then heat-treated at 1050 °C for 24 h for homogenization and furnace-cooled.

2.2 Anodizing treatment

The electrochemical anodization of Ti-xNb alloys were galvanostatically performed using DC power supply (KJPP-5003, KapJin, Korea). A constant-current was maintained by adjusting the voltage.

Prior to the electrochemical treatment, Ti-xNb alloys were polished mechanically to a mirror image. Next, they

were rinsed with ultra-pure water and dried in air at room temperature.

All anodization experiments were carried out at room temperature using two electrodes that were separated by 20 mm. the TiO₂ nano-pore arrays were prepared in a cylindrical electrochemical reactor (60 mm diameter by 60 mm height). A sample was used as anode and a platinum plate was used as cathode. The current density in the cell was 30 mA/cm² for the sample. The electrolysis time was set at 30 min. During the anodization, the electrolytes (1 M phosphate acid) were stirred using a magnetic stirrer. After the treatment, the samples were rinsed in ultra-pure water, dried at room temperature and characterized.

2.3 Characterization of anodized surface

The microstructures of as cast specimens were examined after they had been metallographically polished, and then etched in Keller's reagent with 2 ml HF/3 ml HCl/5 ml HNO₃/190 ml H₂O. Structural characterization of the all samples was carried out with a field emission scanning electron microscope Hitachi FE-SEM S4800. The scanning electron microscope was capable of energy dispersive X-ray spectroscopy (EDX). The phases were analyzed by X-ray diffraction (XRD) at 40 kV and 30 mA. X-ray crystallography was performed using a Ni-filtered Cu K α radiation source. Phases were identified by matching their

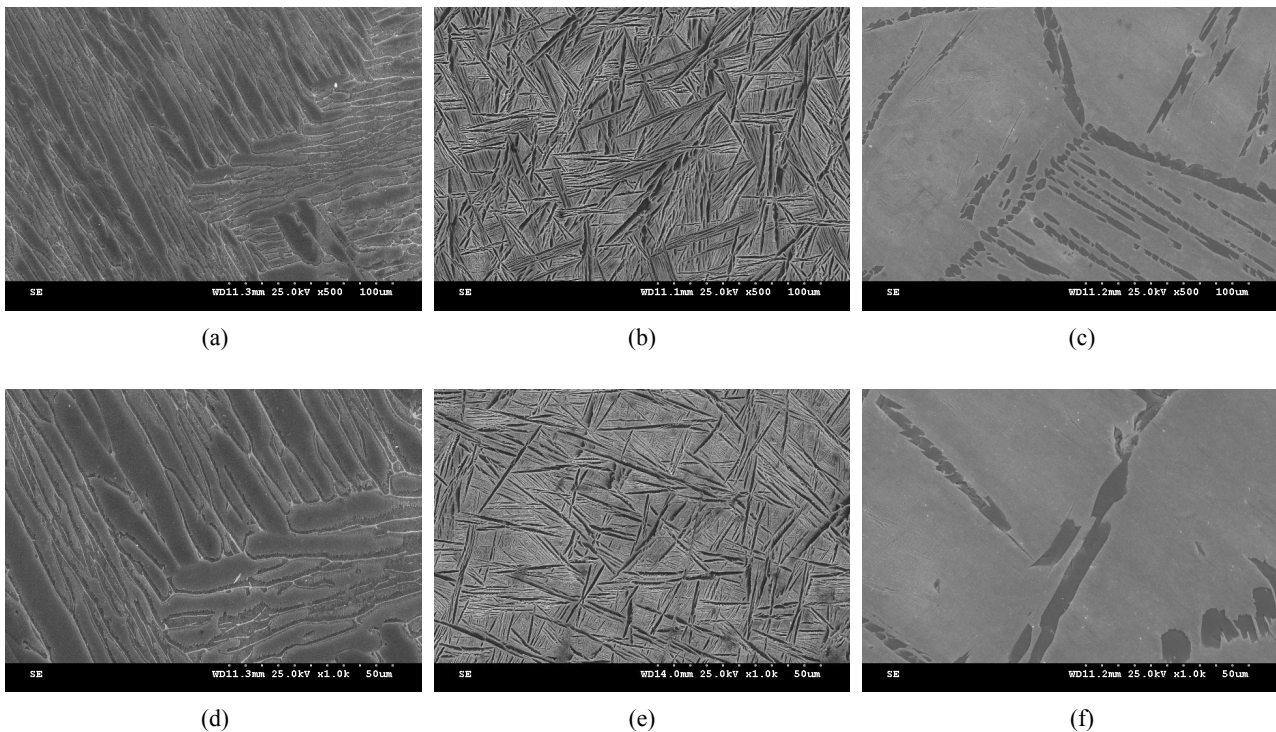


Fig. 1. SEM micrographs showing the surface morphology of Ti-Nb alloys. (a), (d) Ti- 3Nb (b), (e) Ti- 20Nb (c), (f) Ti-40Nb

characteristic peaks with those in the files of the Joint Committee on Powder Diffraction Standards (JCPDS). Surface roughness analysis of anodic TiO₂ films was carried out with a surface roughness tester M.SE-1700, Kasaka, Japan.

3. Results and discussion

The microstructures shown in Fig. 1 are taken from the samples, which were solution treated at 1050 °C for 30 min followed by furnace cooling. Fig. 1 shows the microstructures of Ti-xNb alloys of varying Nb content.

The microstructure of the Ti-3Nb alloys exhibits an equiaxed, as shown in Figure 1 (a, d). Fine needle-like traces of martensite were observed at the prior β grain boundary in the image of Ti-20Nb (Fig. 1 (b, e)). In Ti-40Nb alloys (Fig. 1 (c, f)), no trace of martensite phase is seen assigned to a complete β -phase. The apparent volume fraction of martensite decreased with increasing Nb content in Ti-xNb alloys, as seen in Figure 1. This may be associated with β -phase stability, i.e., the stability of β -phase would be enhanced with increasing Nb content, since Nb is known to be a β -stabilizer. The average composition of the Ti-xNb alloy as measured using EDX in the SEM was Ti-3Nb, Ti-20Nb and Ti-40Nb.

Fig. 2 shows the XRD profiles for three different samples

in which solution treatment was carried out at 1050 °C for 30 min followed by furnace cooling. We prepared three samples, varying Nb content, in order to investigate the alloying element effect on phase formation behavior. The structure of alloy was changed from α -phase to β -phase with increase of Nb content.

The literature reports the use of various electrolytes for the fabrication of TiO₂ nanostructure.¹⁶⁾ However, these

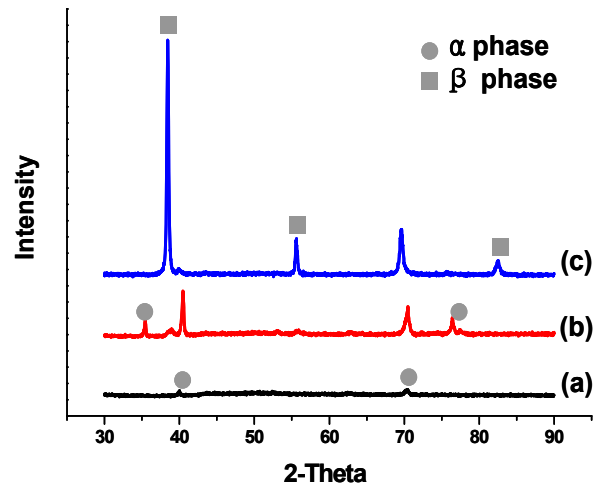


Fig. 2. XRD showing the elements of Ti-xNb. (a) Ti- 3Nb (b) Ti- 20Nb (c) Ti-40Nb

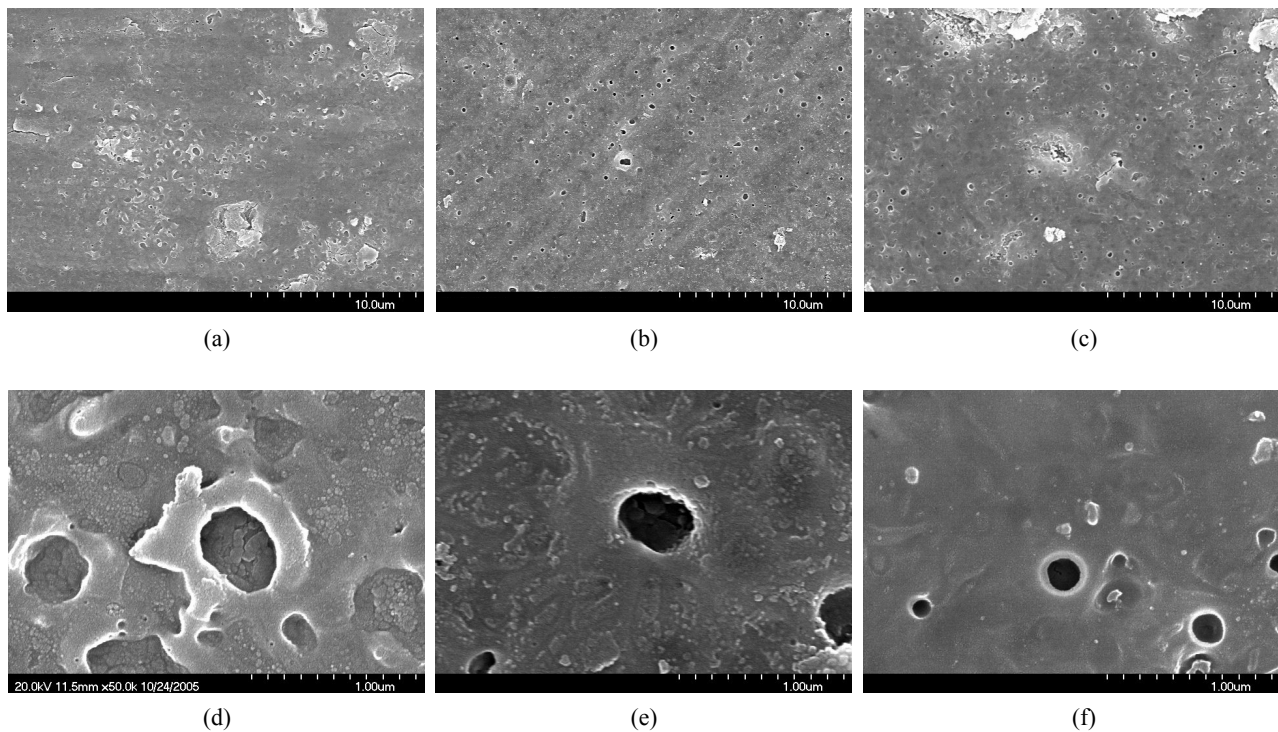


Fig. 3. SEM micrographs showing the surface morphology of anodized alloys. (a), (d) Ti- 3Nb (b), (e) Ti- 20Nb (c), (f) Ti-40Nb

anodization experiments were carried out under constant-voltage conditions and, as a result, the current densities changed greatly during electrolysis (e.g. from 15 to 28 mA/cm²¹⁷). These phenomena may suggest that current density plays a significant role in nanostructure with respect to pore size and morphology. Therefore, a galvanostatic anodization method was used in this work. To obtain the anodic TiO₂ layer an anodic constant current of 30 mA/cm² was applied on titanium surface, and then the anodic potential was increased slowly.

Fig. 3 shows SEM image of surface structures that were obtained with for current densities of 30 mA/cm². As can be seen in Figure 3, the surface of Ti-40Nb is rather smooth. This is also confirmed by roughness test (Table 1) revealing that although the overall surface roughness decreased following anodic oxidation to Ra= 0.2213 μm. SEM and Surface roughness test results, nano-pore size formed on surface and surface roughness decreased as Nb content increased.

Fig. 4 shows the X-ray diffraction (XRD) patterns of the anodic TiO₂ with Nb contents. The anatase phase with

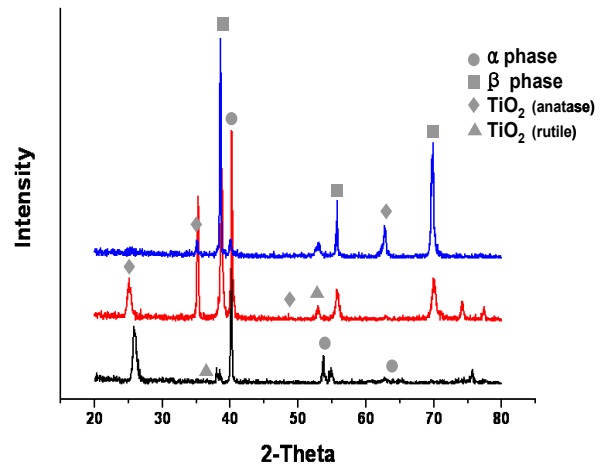


Fig. 4. XRD showing the elements of Anodized Ti-xNb alloys. (a)Ti- 3Nb (b) Ti- 20Nb (c)Ti-40Nb

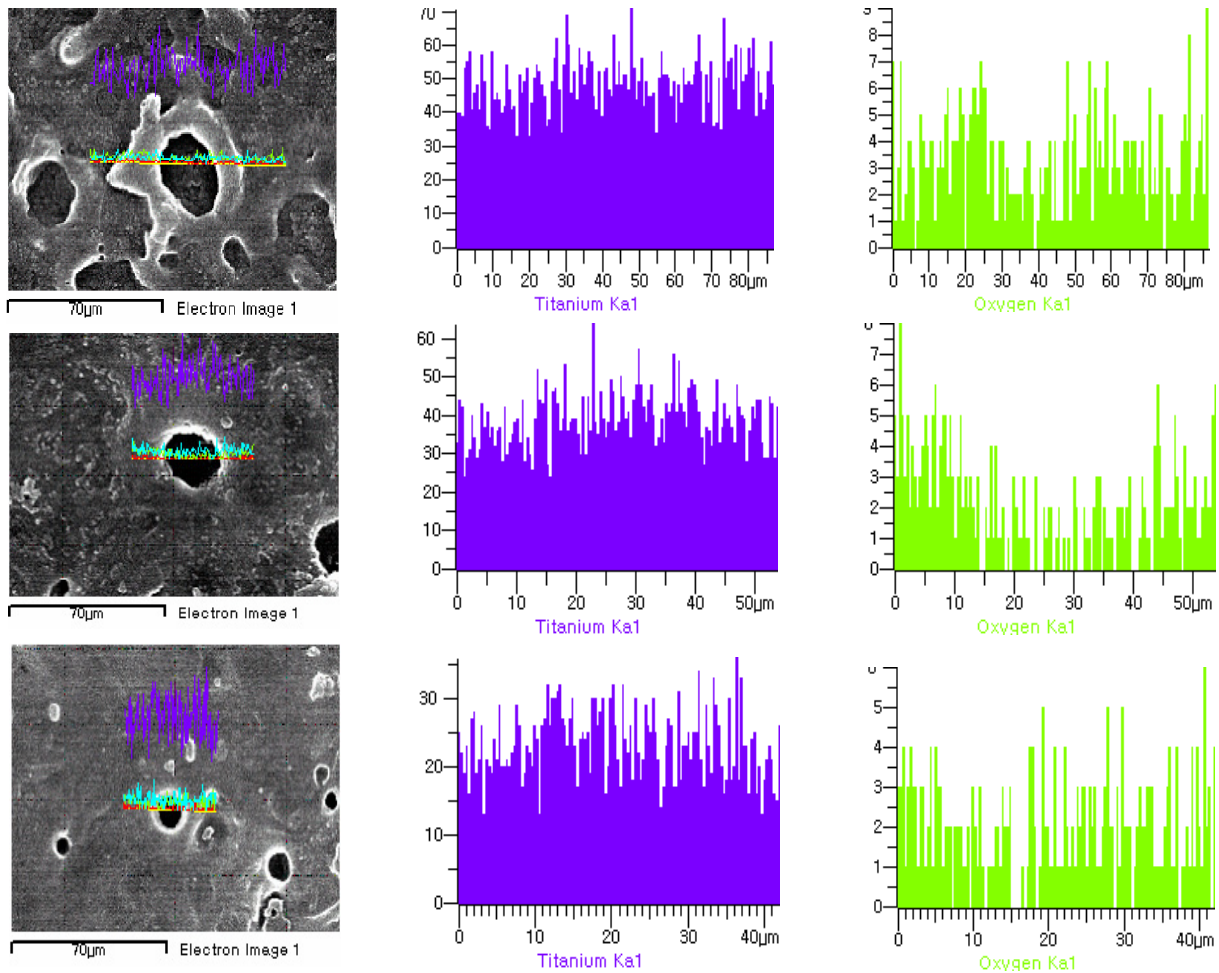


Fig. 5. Line analysis showing elemental distribution of Ti and O for the TiO₂ layer formed at 30 mA/cm² for 30 min. (a) Ti- 3Nb (b) Ti- 20Nb (c) Ti-40Nb

rutile revealed at all stage of anodization from XRD results. It is well known that the TiO₂ has three crystal structures such as anatase, rutile and brookite, and the anatase TiO₂ is more reactive than the rutile.¹⁸⁾ And titanium peak observed in pattern is due to the titanium substrate.

However, no peaks of Nb₂O₅ or other Nb oxide were detected suggesting that Nb atoms are dispersed in TiO₂-based solid solution. It has been previously reported that in the anatase structure at least 20% of Ti atoms can be substituted by Nb.¹⁹⁾ From the result of line analysis, as shown in Fig. 5, intensity of Ti peak was high in the center of pore, whereas, intensity of O peak was high in the outside of pore center. The anodic TiO₂ film formed by electrochemical method has a porous and relatively rough morphology composed of anatase and rutile structure.

4. Conclusions

(1) The structure of alloy was changed from α -phase to β -phase with increase of Nb content.

(2) From XRD results, the structure of TiO₂ formed on the Ti-xNb surface was anatase, intensity of TiO₂ peak decreased as Nb content increased.

(3) Surface roughness test and SEM results, nano-pore size formed on surface and surface roughness decreased as Nb content increased.

(4) From the line analysis results, intensity of Ti peak was high in the center of pore, whereas, intensity of O peak was high in the outside of pore center.

Consequently, as the Nb content increased, porosity size and roughness of oxide films decreased. Also, Ti-Nb alloys showed phase transformation of the α -phases into β -phases.

Acknowledgments

“This work was supported by research funds from KEMCO(2006) and 2nd Stage of Brain Korea 21”

References

1. J. Lausmaa, B. Kasemo, H. Mattsson, and H. Odelius, *Appl. Surf. Sci.*, **45**, 189 (1990).
2. T. Albrektsson, *CRC Crit. Rev. Biocompatibility*, **1**, 53 (1985).
3. A. Wennerberg, T. Albrektsson, and B. Andersson, *Int. J. Oral Maxillofac. Implants*, **11**, 38 (1996).
4. P. R. Klokkevold, R. D. Nishimura, M. Adachi, and A. Caputo, *Clin. Oral Implants Res.*, **8**, 442 (1997).
5. D. Buser, T. Nydegger, T. Oxland, D. L. Cochran, R. K. Schenk, H. P. Hirt, D. Snetivy, and L. P. Nolte, *J. Biomed. Mater. Res.*, **45**, 75 (1999).
6. W. Weng, S. Zhang, K. Cheng, H. Qu, P. Du, G. Shen, J. Yuan, and G. Han, *Surf. Coat. Technol.*, **167**, 292 (2003).
7. W. Weng and J.L. Baptista, *Biomaterials*, **19**, 125 (1998).
8. Q. Chen, F. Miyaji, T. Kokubo, and T. Nakamura, *Biomaterials*, **20**, 1127 (1999).
9. P. Ducheyne and Q. Qiu, *Biomaterials*, **20**, 2287 (1999).
10. A. Nakahira and K. Eguchi, *J. Ceram Process. Res.*, **2**, 108 (2001).
11. E. Kontonasaki, T. Zorba, L. Papadopoulou, E. Pavlidou, X. Chatzistavrou, K. Paraskevopoulos, and P. Koidis, *Cryst. Res. Technol.*, **37**, 1165 (2002).
12. L. L. Hench, *J. Am. Ceram. Soc.*, **74**, 1487 (1991).
13. D. C. Clupper and L. L. Hench, *J. Mater. Sci., Mater. Med.*, **12**, 917 (2001).
14. M. Ninomi, *Mater Sci Eng A*, **243**, 231 (1998).
15. E. Takahashi, T. Sakurai, S. Watanabe, N. Masahashi, and S. Hanada, *Mater Trans*, **43**, 2978 (2002).
16. D. W. Gong, C. A. Grimes, and O. K. Varghese, *J. Mater. Res.*, **16**, 159 (2003).
17. J. Zhao, X. Wang, R. Chen, and L. Li, *Solid State Commun.*, **134**, 705 (2005).
18. M. A. Fox and M. T. Dulay, *Chem. Rev.*, **93**, 54 (1993).
19. Y. Furubayashi, T. Hitosugi, Y. Yamamoto, K. Inaba, G. Kinoda, Y. Hirose, T. Shimada, and T. Hasegawa, *Appl. Phys. Lett.*, **86**, 252101 (2005).